An analytical model for vortex core pinning in a micromagnetic disk

J.A.J. Burgess [a,b,*,1], J.E. Losby [a,b], M.R. Freeman [a,b,*]

[a] Department of Physics, University of Alberta, Edmonton, Alberta, Canada T6G 2E1
[b] National Institute for Nanotechnology, Edmonton, Alberta, Canada T6G 2M9

A B S T R A C T

A two-parameter analytical model is constructed to describe a thin, magnetically soft, circular disk in the vortex state. The model is capable of describing the change in evolution of net magnetization and of vortex core position when the core interacts with a magnetic pinning site. The basis of the two-parameter model is formed by a piecewise, physically continuous, magnetization distribution constructed with two regions described by different one-parameter models. Benchmarking against numerical simulations of ideal disks with and without pinning sites shows that the model provides accurate predictions of magnetization, hysteretic transitions, and 2-D displacement of the vortex core in the presence of pinning sites. The demonstrated accuracy of the model supports its use as an empirical tool to extract quantitative maps of vortex pinning energies from measurements of magnetization.

1. Introduction

Interest in magnetic vortices [1,2] in thin disks has grown dramatically over the past two decades. Topological structures such as vortices are stable, manipulable objects that show promise as logic elements or storage media in spintronics applications [3]. The thin soft magnetic disk, the prototypical system containing a vortex, has therefore been subject to extensive investigation. Properties studied include structure [4,5], dynamical modes [6–8], annihilation [9,10], and creation [9,11–13]. As each aspect of vortex physics is probed experimentally, and considered for technological applications, theoretical understanding via simulation and modeling is also advanced. Modeling is particularly important in the case of the thin ferromagnetic disk as it presents a well-defined system amenable to description by an analytical approach.

Extension of analytical models to include pinning effects has gained increasing importance. The interaction of vortex cores or domain walls with film inhomogeneities has been a topic of significant recent interest. Geometric defects or magnetic impurities can increase or decrease the energetic cost of the topological magnetic structures [14], creating preferential locations for domain walls or otherwise altering the magnetization distribution. In the disk system, direct observations of vortex state pinning have been made with Lorentz microscopy [15] while the effect on vortex gyration has been observed with time-resolved magneto-optical Kerr effect microscopy [16–19] and electronic techniques [20]. Incorporation of pinning potentials into existing analytical models has permitted a qualitative description of the position of the vortex and its reduced displacement susceptibility [21]. This approach, however, is insufficient for quantitative applications. Recent work using nanomechanical torque magnetometry has provided direct observation of the Barkhausen steps associated with jumps in core position [22]. Quantitative analysis of these results necessitates the development and benchmarking of a model that permits a quantitative description of both net disk magnetization and vortex core position in the presence of pinning effects. To accomplish this, the potential for evolution of the magnetic moment of the outer regions of the disk, decoupled from the vortex core position, must be acknowledged. A two-parameter description permits the inclusion of a dipole-exchange spring coupling of the core to a parameterized outer magnetic moment. Presented here is a detailed description of the construction of the two-parameter model and verification of its accuracy against numerical simulations of magnetic vortices in disks featuring pinning sites.

1.1. The vortex state and existing models

In zero field, the vortex state in a disk represents the ground state configuration for a wide variety of disk aspect ratios. Over most of the disk, a circularly symmetric in-plane magnetization distribution maintains magnetization tangential to the disk boundary and reduces dipolar energy. This necessitates a higher exchange energy relative to the uniformly magnetized state, and results in an out-of-plane magnetized core at the disk center

* Corresponding author.
    E-mail addresses: jaburges@ualberta.ca (J.A.J. Burgess),
mark.freeman@ualberta.ca (M.R. Freeman).
    [1] Now at the Max Planck Institute for Structure and Dynamics of Matter, 22761 Hamburg, Germany.

featuring high energy density. For clarity, the in-plane region outside of the core is referred to as the skirt. Analytical models of the vortex state aim to describe the net energy and magnetization in terms of a reduced set of parameters, often vortex core position. This description immediately implies the potential for an empirical ruler to extract core position from magnetization, providing a practical motivation for models with high accuracy.

The zero-field vortex state ansatz was first developed for the magnetic disk by Aharoni [23]. Further work by Usov and Peschany [4] determined an exchange optimized functional form of the core magnetization profile exhibiting good agreement with simulation [24] and experimental observations [5]. Computation of the evolution of the state with field presents a more challenging problem. Extended models built on this initial work use simplifying assumptions to compute magnetization distributions with a displaced core. The Rigid Vortex Model (RVM) considers the displacement of the core under the assumption that the magnetization distribution developed by Usov and Peschany simply translates rigidly relative to the disk boundary, remaining circularly symmetric around the core [25,26]. Magnetization distributions that look more realistic may be computed by minimization of the exchange energy using prescribed boundary conditions; this leads to the so-called Two Vortex Model (TVM) [27,28]. The assumptions about rigidity or boundary conditions lend particular strengths to each type of model: higher order versions of the RVM provide effective descriptions of the magnetic susceptibility of the displaced vortex [10], while the TVM provides a good description of low field vortex core dynamics [29–31]. The RVM and TVM make critical contributions to the two-parameter model discussed here and, therefore, are introduced in the following sections. An additional modification to the RVM is also introduced that significantly improves its performance.

2. Theory

2.1. The rigid vortex model

The RVM is derived by considering the zero field vortex magnetization distribution [23,4] to be immutable, and then translating that distribution relative to the physical boundary of the disk [25,26] (Fig. 1). To solve the model, the energetic contributions from demagnetization charges, exchange and the applied field must be computed in terms of the core position. Here, a soft anisotropy free material will be considered. In terms of the reduced field, $h = H/M_S$, the 3rd order expression for the total normalized energy of a disk with a radius R and thickness L described by the RVM [10] may be expressed as

$$\frac{E_{tot}}{\mu_0 M_s^2 V} = \frac{\beta}{2} b^2 - h\left(b - \frac{b^3}{8}\right), \qquad (1)$$

where the normalized core displacement $s = \Delta r/R$ is equal to b, V is the disk volume, $\beta = F(L,R) - R_o^2/R^2$ is a constant describing the demagnetization energy and exchange energy with $R_o = \sqrt{2A/\mu_o M_S^2}$ denoting the exchange length. In the derivation of the RVM, the factor $F(L,R)$ is found to be equal to the demagnetization factor for a disk uniformly magnetized in plane [25].

Some consideration must be given to this factor in the context of a disk made of a soft magnetic material. Any inspection of displaced vortex magnetization distributions in simulated disks composed of permalloy or a similar soft material reveals the rigid assumption is flawed (Fig. 2). The magnetic moments near the boundary of the disk will always rotate to a certain degree to partially maintain a tangential boundary condition and lower the
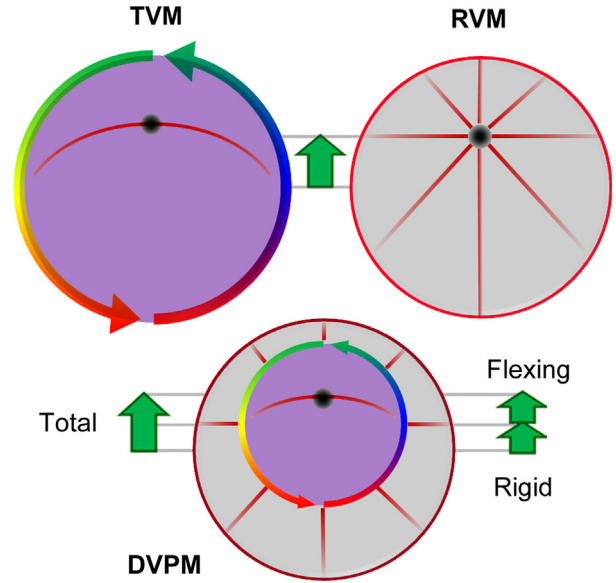

Fig. 1. Schematics depicting the evolution of the magnetization distribution as the vortex core is displaced for various analytical models. The red lines indicate contours of constant $|M_y|$ magnetization while the color gradient circular arrows indicate an in-plane tangential boundary condition for the magnetization. The TVM holds a tangential boundary condition as the vortex core is displaced. The RVM simply translates the circularly symmetric zero field magnetization distribution relative to the disk. The DVPM incorporates a central flexible TVM-described region into an RVM-described annulus in creating a piecewise continuous magnetization distribution. Major energetic contributions arise from the demagnetization charges computed in each model. In the TVM, only volume demagnetization charges are present (purple shading). In the RVM, only edge demagnetization charges are accounted for (red line). In the DVPM both are present. Consequently, since the RVM parameterizes all demagnetization charges as edge charges, the computed density of edge charges of the RVM annulus must be modified for use in the DVPM. (For interpretation of the references to color in this figure caption, the reader is referred to the web version of this article.)
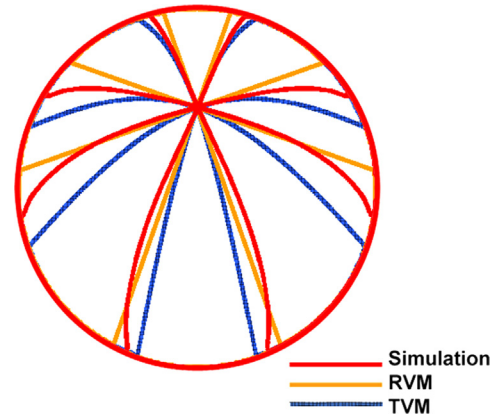

Fig. 2. Contours of constant magnetization aid visualization and comparison of the magnetization distributions predicted for a displaced vortex core by the RVM and the TVM with no side charges, against simulation. Of critical importance is the fact that the TVM contours lag behind the contour lines of the simulation everywhere, indicating an underestimate of the total magnetic moment. By contrast the RVM contours lead and lag the simulation contours, indicating a smaller error in the computed total magnetic moment. Here the contours for $|M_y/M_S| = 0.4$ and 0.8 are shown, compared against a simulation for a disk with a diameter of 1 μm, and thickness of 40 nm. (For interpretation of the references to color in this figure caption, the reader is referred to the web version of this article.)

total demagnetization energy by redistributing uncompensated edge dipoles into the volume. In computation of the energy of uniformly magnetized particles, it is possible to account the net reduction by solving for the magnetic potential at the disk boundary taking into account a discontinuity in the rotational susceptibility of the material inside and outside of the disk. The

correction is applied only to the energy and does not explicitly compute the deformation of the magnetization. This correction is known as the μ^* correction [32,33], and results in a constant factor applied to reduce the demagnetization energy that is incorporated into the demagnetization factor.

For a disk in the vortex state, the rigid assumption places demagnetization charges exclusively on the disk perimeter. Locally, the symmetry of uniform magnetization at a boundary is maintained, and it is therefore possible to compute the same factor for the reduction in demagnetization energy as in the uniform case. The amount that the μ^* correction reduces the demagnetization energy is dependent on the rotational susceptibility of the material. For a low anisotropy, soft material such as permalloy, the effective susceptibility is very high. Relative susceptibilities > 100 provide approximately the same reduction as an infinite value [34]. For comparison, approximating a relative susceptibility of ~ 49 (equal to that of iron [32]) as infinite would yield only a $< 0.8\%$ error in the correction for an iron disk. Consequently, when considering soft, low anisotropy disks, it is reasonable to replace the factor $F(L,R)$ in Eq. (1) with a corrected demagnetization factor, $F_c(L,R)$, computed for an infinite value of the susceptibility. The value of $F_c(L,R)$ may be computed rigorously [34], and remains a fixed parameter for a given disk size. No additional fit parameter is introduced.

Solving the RVM permits calculation of the vortex displacement as a function of field, $b_o(h) = (-4\beta + 2\sqrt{4\beta^2 + 6h^2})/3h$, and the magnetization $m_o(h) = M_o(h)/M_S = b_o - b_o^3/8$. Note that removing the third order term in the magnetization, and consequently the external field energy contributing to $b_o(h)$, reduces the model to the second order RVM [25,26] with $m_o(h) = b_o(h) = h/\beta$.

The application of the susceptibility correction may be verified by comparing the RVM predictions made using a corrected demagnetization factor against simulation and computations using an uncorrected value. Without correction, the energetic cost of vortex displacement is too large and the RVM offers a poor prediction of both vortex position and magnetization as a function of field (Fig. 3). By comparison, with correction, the RVM provides excellent estimates and serves as a useful tool for predicting both quantities in ideal disks. In other words, the RVM provides a good estimate of the net magnetization as a function of core displacement, and to create a useful model, only the energetic cost of displacement must be adjusted.

2.2. The two vortex model

The TVM is derived by setting a boundary condition and computing the magnetization distribution that minimizes the exchange energy for a given vortex core displacement [27,35]. The most widely used version of the TVM permits no demagnetization charges on the disk boundary [27,29]. This forces all demagnetization charges to be redistributed into the volume of the disk, significantly reducing the demagnetization energy, and also introducing prominent warping of the circular symmetry in the skirt magnetization. For disks with a radius significantly larger than the core radius, contributions from the core may be neglected [27]. In the same form as used for the RVM, the total normalized energy may be written down to second order for a large disk as described by the TVM:

$$\frac{E_{tot}}{\mu_0 M_s^2 V} = \frac{\alpha}{2}a^2 - \xi ha, \qquad (2)$$

where the normalized core displacement $s = \Delta r/R$ is equal to $a/2$, $\alpha = RF_1(L,R)/L - R_o^2/2R^2$ incorporates the demagnetization energy and exchange energy, and ξ is a constant ($\sim 10/29$). The function $F_1(L,R) \sim k(L/R)^2$ with $k = 0.08827$, is an equivalent demagnetization factor describing the volume magnetostatic charges resulting from
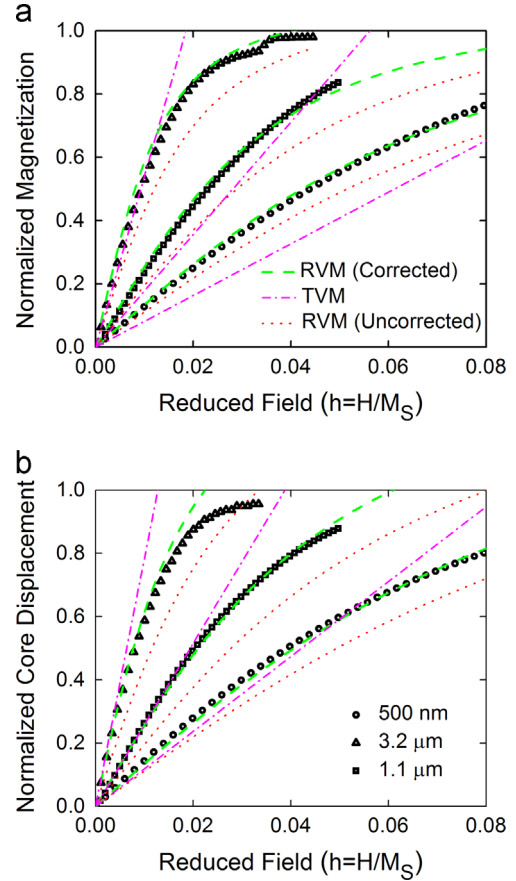

Fig. 3. Computation of magnetization (a) and vortex core displacement (b) as a function of field is compared against simulation for the RVM, the susceptibility corrected RVM, and the TVM with no side charges. The uncorrected RVM provides poor estimates of both quantities for the three simulations shown. By comparison, the corrected RVM provides excellent estimates of both quantities. The TVM provides good estimates of the core displacement, but for disks in the experimentally pertinent ($\sim \mu$m) size range, provides an underestimate of the magnetization. (For interpretation of the references to color in this figure caption, the reader is referred to the web version of this article.)

flexing of the magnetization distribution. As before, minimization with respect to a allows computation of $a_o(h) = \xi h/\alpha$ and magnetization $m_o(h) = \xi a_o(h)$.

The TVM with a tangential boundary condition over-enforces the elimination of perimeter demagnetization charges. Consequently, though it appears more realistic than the RVM when compared to simulation, the computed magnetization distribution is still incorrect (Fig. 2). In particular, the pinning of the magnetization of the boundary suppresses the relatively large magnetic moment that may develop near the disk edges as the core is displaced by field. This leads to a systematic underestimate in the magnetization as a function of applied field (Fig. 3). The TVM, however, does provide a reasonably accurate computation of core displacement as well as excellent predictions of core dynamics [29,7,30,31].

2.3. Effects of pinning

In the presence of a pinning site the vortex core position is no longer dictated solely by torques exerted on the core by the surrounding in-plane magnetization distribution. The pinning sites create preferential locations for the core within the disk. When the core is in a preferential site, the energy cost of further core displacement is increased and this necessarily influences how the magnetic moment in the skirt will evolve. Under increasing
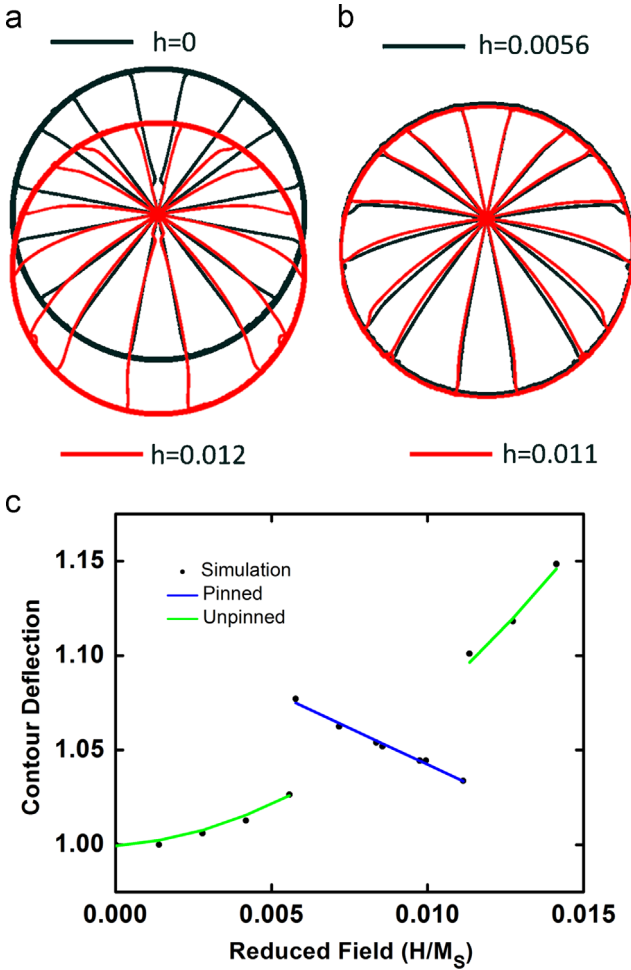
Fig. 4. (a) Contours of constant $|M_y|$ value are computed from a simulation for two different fields and overlaid such that the vortex core positions overlap. (b) The same type of plot is produced for the core trapped in a pinning site. The pinned contours qualitatively shift in the opposite direction between low field and high field, compared to case (a). (c) The normalized and averaged angular deflection of contours is shown as a function of field as the core moves through the pinning site. The angles are measured between the vertical ($|M_x| = 1$) line and the intersection of the contours with a circle of radius $R/2$ centered on the vortex core. This reflects the net deformation of the magnetization distribution inside of $R/2$. For a pinned core and increasing field, the angular deflections reduce, partially restoring the circular symmetry of the zero field vortex state. (For interpretation of the references to color in this figure caption, the reader is referred to the web version of this article.)

field, the magnetization of the disk will continue to grow despite the pinning. This results in the magnetic moment away from the core increasing preferentially.

Examining the angular deflection of contours of constant magnetization in a simulation makes the behaviour of the pinned magnetization distribution easier to picture. The contours exhibit a deflection with a non-monotonic evolution as the vortex traverses the pinning site (Fig. 4). During pinning, the contours begin to return to the original (zero field) angles of deflection, partially restoring the circular symmetry of the magnetization distribution. This contrasts to contour evolution in an ideal (pinning site free) disk, where the angle of deflection changes monotonically with core displacement.

The change in deformation represents a significant energetic influence on the core. The flexible nature of the magnetization distribution acts as a combined dipole-exchange spring. The spring can absorb energy, allowing a core to jump ahead to a preferential site. Similarly, stored energy lowers as the core is trapped in the pinning site, permitting the core to stay in the site longer. This has

a prominent effect on observed hysteresis in pinning sites, as well as on computation of depinning energy barriers.

Both the RVM and TVM link the computed model magnetization directly to the vortex core displacement in the disk using only a single parameter.[2] This limitation renders the models incapable of computing, or even qualitatively describing the non-monotonic evolution of the deformation. However a combination of these two models may be constructed, modeled after the observed magnetization distribution, and incorporating both rigid translation and flexible deformation.

2.4. The deformable vortex pinning model

The correct computation of the net magnetic moment of a disk containing a displaced vortex becomes particularly important when considering the use of a field to push a vortex core through a pinning potential. The goal is then to construct a model that incorporates the accurate computation of the magnetic moment in the outer regions of the skirt, as featured in the corrected RVM, along with a flexible component that allows this magnetic moment to be decoupled from the vortex position. This is the approach followed here by use of a piecewise model that we call the Deformable Vortex Pinning Model (DVPM). In the DVPM, the disk is divided into two circularly symmetric regions. An outer annular section described by the RVM surrounds an inner section described by the TVM with a no side charge (tangential) boundary condition. The outer section translates rigidly. The inner section translates along with the outer annulus while also providing deformation. The tangential boundary condition ensures that the magnetization distribution remains piecewise continuous. The outer RVM annulus parameterizes the dominant magnetic moment developed in the outer regions of the disk, while the flexible TVM center parameterizes the dipole exchange coupling between this outer moment and the core. The use of the RVM for the outer ring is motivated by its accuracy in computing the magnetic moment. It is therefore used for the section of the disk that contributes the largest magnetic moment. Inside, the TVM with no side charges must be used to preserve piecewise continuity in the magnetization distribution.

With the two contributing models introduced, the DVPM may now be constructed. The disk radius remains R, while the radius of the inner region will be denoted R_1. As with the RVM and TVM, magnetocrystalline anisotropy is neglected. The total energy of the combined piecewise model may be written down in terms of the energies of the two component models:

$$\frac{E_{tot}}{\mu_0 M_s^2 V} = \frac{\beta'}{2} b'^2 - h \left(b' - \frac{b'^3}{8} \right) + \gamma \left(\frac{\alpha'}{2} a'^2 - \xi h a' \right), \tag{3}$$

where b' is the normalized displacement of the outer RVM shell, and $a'/2 = \Delta r_1/R_1$ is the central TVM core displacement normalized to R_1. The factor $\gamma = R_1^2/R^2$ scales the energy contributions of the central region according to its size. The total core displacement is $s = \Delta r/R + \Delta r_1/R = b' + R_1 a'/2R$. The corresponding normalized magnetization is $m = b' - b'^3/8 + \gamma \xi a'$. The factors β' and α' describe the demagnetization and exchange energies of the annulus and central region respectively as β and α did for the RVM and TVM. For the inner region $\alpha' = R_1 F_1(L, R_1)/L - R_o^2/2R_1^2$. For the annulus, β' requires careful consideration. The corrected RVM computes the correct energy cost of vortex displacement in the absence of pinning. It is clear that simply adding an independent flexible region will disrupt the parameterization of the magnetization

---

[2] The TVM uses a second parameter to describe distortions of the core profile under deflection, however this parameter does not have a significant influence on the overall disk magnetization or core displacement. It is therefore unsuitable for describing the influence of the skirt magnetization on the core.
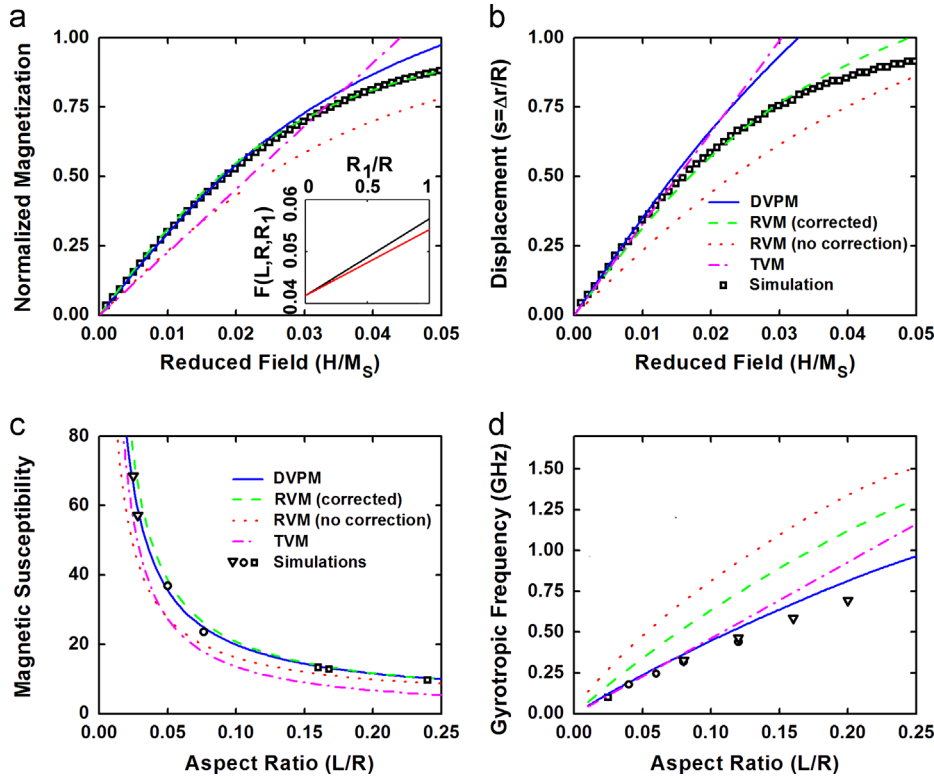
Fig. 5. (a) The computed m–h curves from four models (RVM corrected and uncorrected, DVPM, TVM) are compared against a simulation of a 1 μm diameter, 30 nm thick disk with $M_S = 800$ kA/m. (b) The computed normalized vortex displacement as a function of field is compared against the simulation. The legend inset in panel (b) applies to both (a) and (b). Only the RVM with a susceptibility-corrected demagnetization factor and the DVPM describe both position and magnetization accurately for displacement $s < 1/2$. Inset in (a) is a comparison of corrected demagnetization factor as a function of R_1 used in the DVPM computed by interpolation (solid red) and from demagnetization energies (black). (c) The computed initial susceptibility is compared against simulation for disks of varying radius (R) and thickness (L). Squares denote $R = 250$ nm, circles $R = 500$ nm, and triangles $R = 1800$ nm. All simulations use $M_S = 800$ kA/m except the $R = 1.8$ μm which used $M_S = 715$ kA/m. (d) Using the same simulation parameters, the frequency of the gyrotropic mode was computed. The legend in (c) applies to panel (d) as well. Only the DVPM agrees well with both the initial susceptibility and the gyrotropic frequency. For (c) and (d) calculations were performed holding $R = 500$ nm with variable thickness. All DVPM calculations in panels a-d use $R_1 = R/2$. (For interpretation of the references to color in this figure caption, the reader is referred to the web version of this article.)

and energy, resulting in susceptibilities (magnetic and positional) that are too large. Since the dominant energetic contribution arises from the demagnetization energy, it follows that, in order to preserve the total energetic cost of vortex displacement, the demagnetization cost of rigid translation of the annulus should be increased. Scaling the demagnetization energy of the central region suggests that the demagnetization factor of the outer shell requires an increase of $(R_1/R)^2(2R_1/L)F_1(R_1, L)$ for a central region of radius R_1.

The physical meaning of the increase in the shell demagnetization factor may be elucidated by considering it in the context of the susceptibility correction. Effectively, the susceptibility correction permits the RVM to parameterize the reduced demagnetization energy and increased displacement of the vortex core arising due to flexing of the magnetization distribution. Inclusion of a flexible central region explicitly accounts for some of the flexing and demagnetization energy over the disk (Fig. 1). Hence, in the DVPM, some of the change is accounted for, consequently the susceptibility correction should be decreased. Indeed, comparing a linear interpolation between the corrected (F_c) and uncorrected (F_{nc}) demagnetization factors of the form $F(L, R, R_1) = (1 - R_1/R)F_c(L, R) + (R_1/R)F_{nc}(L, R)$ to the estimated change in the RVM shell demagnetization factor described previously shows that the deviation between the two does not exceed 10% over the range $R_1/R = 0$ to 1. This corroborates the application of susceptibility correction and its physical interpretation in the context of a rigid model. The factor β' is then $\beta' = F(L, R, R_1) - R_o^2/R^2$ where the annular demagnetization factor is either $F(L, R, R_1) = (1 - R_1/R)F_c(L, R) + (R_1/R)F_{nc}(L, R)$ or $F(L, R, R_1) = (1 - R_1/R)F_c(L, R) + (R_1/R)^2(2R_1/L)F_1(R_1, L)$ depending on the choice of using the

analytic estimate of the demagnetization increase, or the susceptibility correction interpolation. Here interpolation is chosen over the analytic estimate of the rebalancing energy to maintain the limiting values at the susceptibility-corrected demagnetization factor and the uncorrected value.

Solving the model is a simple matter of computing the optimal values of b' and a' as a function of field. In the ideal disk case, the optimal solution reduces to the decoupled solution for each section separately with the same expressions for $b'_o(h)$ and $a'_o(h)$ as before for the RVM and TVM, but with β' and α' replacing β and α respectively.

Only one free parameter remains, the radius of the inner TVM section. The influence of R_1 is mitigated by the R_1 dependence of the demagnetization factor used for the annulus, however the choice of R_1 is not entirely arbitrary. The constructed model can behave as the RVM in one limit ($R_1 = 0$), or the TVM in the other limit ($R_1 = R$). Consequently, the model can exhibit the failings (and successes) of the RVM in one limit, and the TVM in the other. Optimal computation of the properties, including good prediction of the magnetization as a function of core position and dynamical modes, of the vortex state require an intermediate R_1. This can be estimated by minimizing the deviation of the DVPM from the successful predictions of the RVM ($m(h)$, $s(h)$) and the TVM (gyrotropic frequency). In general, a reasonable agreement with all three parameters can be found for R_1 values of approximately $R/2$. In more detail, the optimal R_1 has a weak dependence on the radius of the disk. Computation of the relative differences between the DVPM predictions and those of the two other models permits identification of a solution for R_1 that maintains good agreement for all three metrics simultaneously. For example, for disks of varying
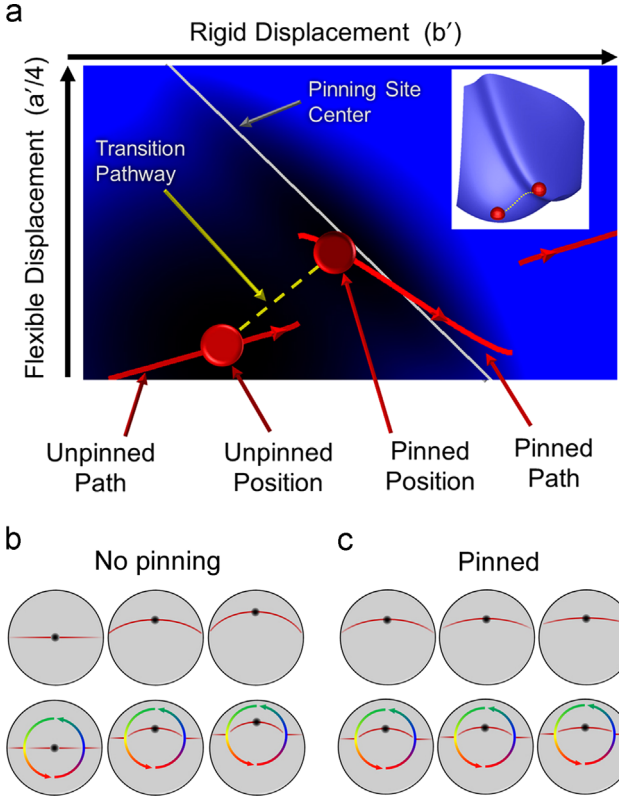
Fig. 6. The DVPM is solved in a 2-D energy space with axes for rigid displacement of the RVM annulus (b') and flexible displacement inside the central TVM region ($a'/4$ for $R_1 = R/2$). (a) A 2-D plot of the energy landscape (color gradient) in the DVPM computed for a 1 μm diameter, 40 nm disk is shown for a fixed field value of $h=0.025$ using an $M_S=800$ kA/m. This is the 2-D landscape that must be solved to find the lowest energy combination of b' and $a'/4$ for a particular vortex displacement. The energy landscape chosen features a single pinning site at $b'+a'/4 = 0.21$. At $h=0.025$, two local minima exist, one inside the pinning site, one outside. As field is changed, the positions of these minima shift along the paths displayed above, allowing the DVPM to describe flexing and rigid displacement in unpinned and pinned situations. Inset at top right is a 3-D representation of the potential at $h=0.025$, the two local minima and the transition pathway. (b, c) The schematics depict the field evolution of the deformation in magnetization distribution using the $|M_y| = 1$ contour of a simulated disk (at top) and the DVPM (at bottom). (b) shows the no pinning case and (c) a case with strong core pinning. Note that in both the simulated and DVPM case, deformation (flexing) decreases when the core is pinned, and increases when it is unpinned. This matches the computed pathway evolution shown in panel (a). (For interpretation of the references to color in this figure caption, the reader is referred to the web version of this article.)

radius between 200 nm and 2000 nm with thickness 40 nm, a solution $R_1 = R(0.6-(5/3)(L/R))$ maintains less than 10% difference in the DVPM predictions for the initial magnetic ($\chi(h=0)$) and positional ($ds(h=0)/dh$) susceptibilities compared to the RVM and the DVPM prediction for the gyrotropic mode compared to the TVM. Deviating from this solution for $R_1(R)$ results in a rapid increase in the relative difference of at least one of the DVPM predictions, indicating that it is close to the optimal choice of R_1 for general application of the DVPM. This semi-analytic method of computing a suitable R_1 value provides a useful starting point for comparison of analytic predictions and simulation.

3. Results

3.1. Application to the ideal disk

From Eqs. (1) to (3) the ideal disk behaviour of each model may be computed and compared to Landau–Lifshitz–Gilbert

micromagnetic simulation.[3] To mimic quasistatic behaviour, time integration with a damping factor of 1.0 was used. All simulations were performed on a 2-D 5 nm × 5 nm × thickness grid using an exchange stiffness constant of 1.05×10^{-11} J/m, with M_S values between 700 kA/m and 800 kA/m and 20 nm, 30 nm or 40 nm thickness. All calculations with the model used an exchange length of 5.85 nm and M_S values matching the simulations.

Comparison of the $m(h) = M(H/M_S)/(\mu_o M_S V)$ and $s(h) = \Delta r(H/M_S)/R$ curves are shown in Fig. 5a and b. Clearly the susceptibility-corrected 3rd order RVM provides the best estimate of both magnetization and vortex displacement as a function of field, while the uncorrected version exhibits the poorest performance. Both the DVPM and TVM provide good estimates of vortex position with field for displacements up to displacements of $R/2$, but of the two, only the DVPM simultaneously gives a good description of the magnetization.

Two other metrics have been applied to evaluate the performance of the analytical models near zero field in past work: initial susceptibility, and the frequency of the lowest order excitation mode of gyrotropic vortex motion. Both of these parameters primarily depend on the aspect ratio of the disks. Initial susceptibility is easily calculated from $m_o(h)$ for each model. Using the collective coordinate approach [36], it may be shown that the gyrotropic mode frequency is $f_o = \kappa/2\pi G$ where $G = 2\pi L M_S/\gamma_o$ with $\gamma_o = 1.76 \times 10^{11} s^{-1} T^{-1}$, and $dE_{tot}/dr = \kappa r$ [29]. For the RVM and TVM, κ is β and 4α respectively. For the piecewise combined model, κ may be computed in the unpinned and zero field case:

$$\kappa = \frac{4(\alpha' + \gamma \xi^2 \beta')\beta'\alpha'}{(2\alpha' + \rho \xi \beta')^2}. \tag{4}$$

Comparisons between simulation and computed results for initial susceptibility and gyrotropic mode frequency are shown in Fig. 5c and d. Dynamic simulations were performed using a realistic damping factor (0.02) but otherwise matched the parameters used in the previous simulations. The poor performances for magnetization description of the TVM and uncorrected RVM manifest as incorrect estimations of the initial susceptibility. However, both approach the simulation results for squat disks, corroborating previous results [25,29] and demonstrating the general utility of these models. By comparison, the DVPM and corrected RVM provide excellent estimates of initial susceptibility for all aspect ratios investigated. Previously, only the TVM has provided reasonable estimates for the gyrotropic frequency of the vortex state while the RVM has provided poor estimates. The success of the TVM is reproduced here, as is the failure of the uncorrected RVM. The susceptibility correction improves the RVM prediction, however it fails to match the performance of the TVM in the prediction of f_o. However, the DVPM provides comparable performance to the TVM for low aspect ratios and improved performance with more squat ideal disks.

3.2. Application to a single pinning site

Having demonstrated the performance of the piecewise model in a perfect disk, pinning may now be considered. Adding pinning to the models is accomplished by adding functions of the form $E_p(b'+R_1a'/2R - X_p)$ for a pinning site located at X_p to Eq. (3), or of the form $E_p(b-Xp)$ for the RVM in Eq. (1). For the RVM case, simply solving for the minima in energy permits a full solution of the problem. For the DVPM, in pinning situations the solution for b' and a' no longer reduce to the solutions for each component independent of one another. Plotting the total energy including
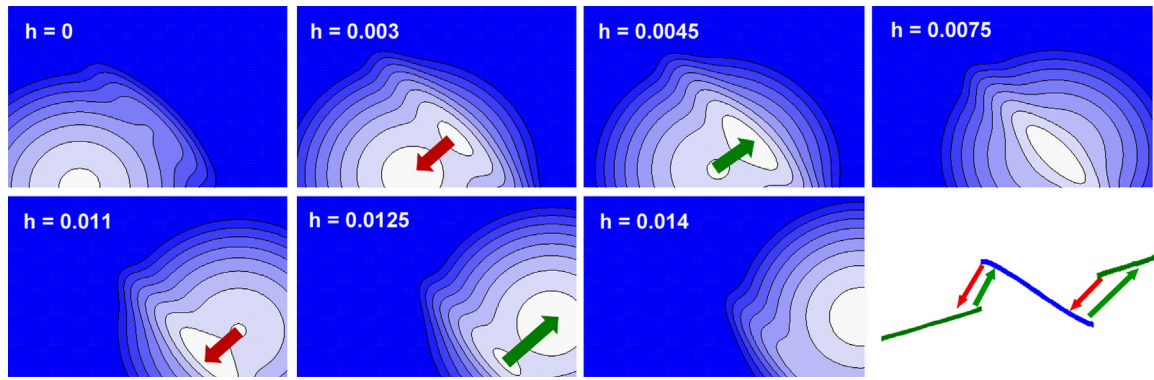

Fig. 7. Plotting the 2-D energy using contours in a' b' space (y and x axes respectively) as a function of reduced field h shows how the vortex core location evolves in both coordinates. Shown above are panels computed for various fields using the same 1 μm diameter, 40 nm disk with a single pinning site shown in Fig. 6. Transitions occur over saddle points between bistable states. Asymmetry in the transition path barrier leads to hysteresis in inter-state transitions for up and down field sweeps. Green arrows denote transitions on the up sweep, red arrows indicate those that occur on the down sweep. The bottom right panel shows the overall path followed by the vortex core in a' b' during a field sweep. (For interpretation of the references to color in this figure caption, the reader is referred to the web version of this article.)
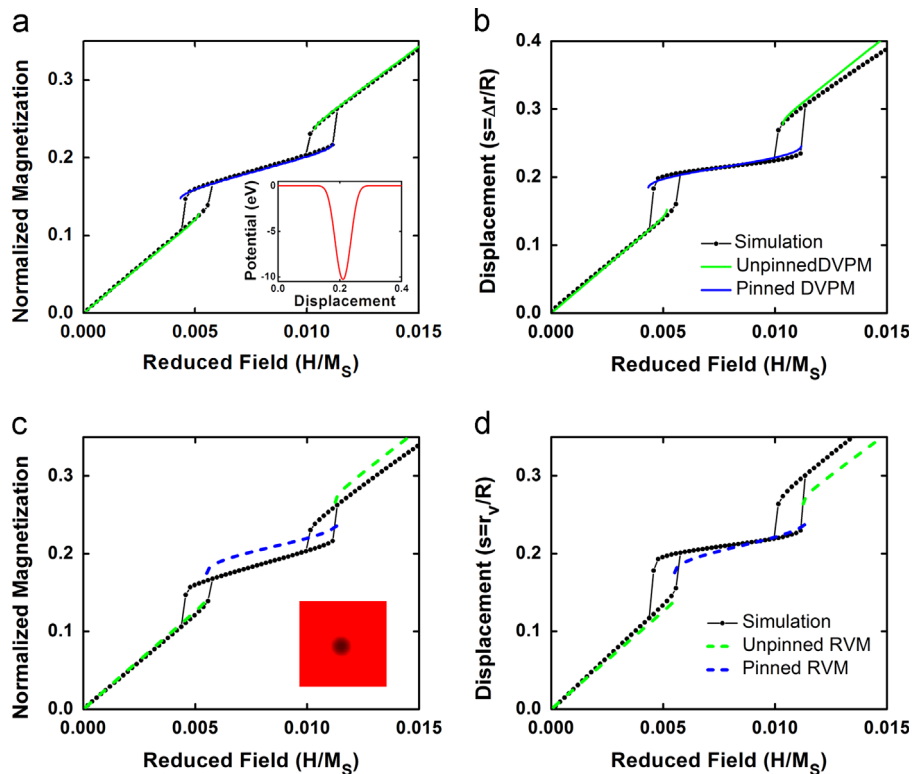

Fig. 8. The m–h (a) and s–h (b) curves for a field sweep up and down are compared against simulation for a 1 μm diameter, 40 nm thick disk with a single pinning site located at 105 nm with an energy profile estimated from the simulation (inset in (a)). For comparison, the same pinning site is added to the susceptibility corrected, one parameter RVM. The computed m–h (c) and s–h (d) curves provide much worse agreement including a larger ((> 10 nm) positional error, and more importantly, a complete absence of hysteresis on entrance and exit from the pinning site. In the simulation the pinning site is included as a region of suppressed M_S (inset in panel (c)) with diameter 40 nm, where at the center M_S=550 kA/m. (For interpretation of the references to color in this figure caption, the reader is referred to the web version of this article.)

field in 2-D b'-a' space provides a direct visualization of the problem (Fig. 6). A full 2-D optimization is required.

In b'-a' space, pinning sites appear as linear troughs (Fig. 6). This permits a simplification of the optimization process by the consideration of pinning site coordinates defined by $b' = i \sin(\theta) + j \cos(\theta)$ and $a' = i \cos(\theta) - j \sin(\theta)$ for $\theta = \tan^{-1}(2R/R_1)$. Switching to i and j coordinates allows independent minimization and simplifies the problem. The position and existence of local minima inside and outside of pinning sites evolves with changing applied field (Fig. 7). Sometimes bistable states exist, and when they do so, there is inevitably a transition pathway between the two extant minima that passes over a saddle point. Applying a 2-D

optimization repeatedly while changing the field permits computation of the values of b' and a' for all minima and saddle points. This in turn permits computation of the quasistatic pinned and unpinned magnetization and vortex position, while locating the saddle points separating minima allows computation of the energy barriers separating bistable states. The critical feature of this minimization process is that the coordinate a may evolve non-monotonically with increasing field, matching the qualitative non-monotonic evolution of the flexing of the magnetization distribution visible in simulation.

Micromagnetic simulations were used evaluate the pinning performance of the DVPM and, for comparison, the corrected RVM.
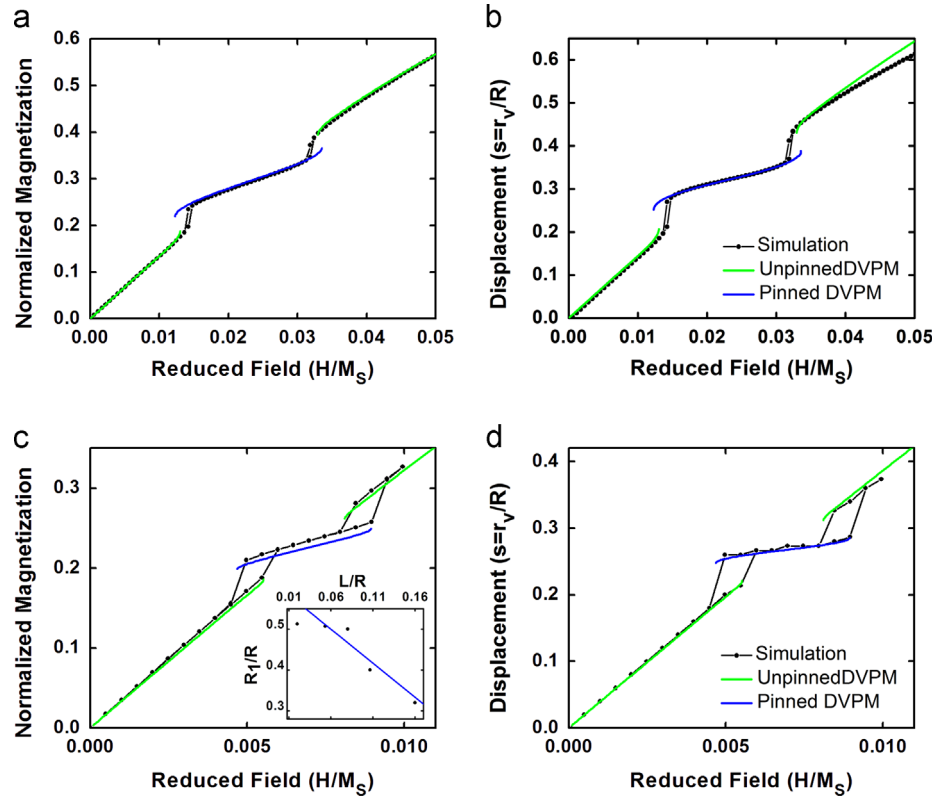
Fig. 9. (a) The DVPM m–h result is compared to a simulation of a 500 nm diameter, 40 nm thick disk with $M_S = 700$ kA/m and a single pinning site located 80 nm away from the center. (b) The computed normalized displacements are compared for the same simulation. For this comparison with $R = 250$ nm, $R_1 = 80$ nm provides the best estimate of hysteresis loop width. The inset shows a plot of the optimal R_1 value found by comparison to simulation as a function of aspect ratio (black points). The blue line is the optimal R_1 value computed by minimizing deviation of the DVPM from the RVM and TVM for initial susceptibility, ds/dh and gyrotropic mode computed for 40 nm thick disks. (c) Comparison to a simulated 1500 nm diameter, 40 nm thick disk with a single pinning site at 200 nm from center shows that the DVPM begins to underestimate the magnetization as disk size increases. (d) The computation of the vortex position and hysteresis loop width remains accurate. For $R = 750$ nm, an R_1 value of 375 nm was used. (For interpretation of the references to color in this figure caption, the reader is referred to the web version of this article.)

Quasi-static simulations were run as described previously using the same parameters as were used for ideal disks. Pinning sites are mimicked using approximately circular regions of depressed saturation magnetization to modify the energy landscape of the disk (Fig. 8c inset). This leads to two contributions to pinning energy, the reduced exchange energy of the core in the low M_S region, as well as reduced demagnetization energy when the core is centered on the site. From the simulation the depth of the energetic profile of the pinning site can be approximated by considering the convolution of a 2-D Gaussian at various offsets with the profile of the M_S variation (Fig. 8a, inset). The Gaussian effectively approximates the exchange energy density of the core, as well as the M_z profile, providing an estimate of how the two energy contributions change as the core shifts relative to the pinning site. Here a full width half max of 17.2 nm is used for the Gaussian approximation. To check that the simulations accurately treated core deformations, supporting simulations were run using reduced 2.5 nm × 2.5 nm and 1.25 nm × 1.25 nm simulation grids. No significant differences were noted.

The performance of the DVPM in describing pinning can be evaluated by three metrics: the pinning site position error, the width of the minor hysteresis loops associated with pinning and depinning, and the combined computed pinned differential magnetic and positional susceptibilities. Fig. 9a–d shows results for a 1 μm diameter, 40 nm thick, disk compared to the DVPM and the 3rd order RVM. The DVPM accurately captures both differential susceptibilities while the RVM fails to capture the positional slope. Both models feature effective position shifts of the pinning site. The DVPM agrees best with the simulation for a pinning site shifted 2.5 nm further from center than the actual simulation

(107.5 nm instead of 105 nm), while a shift greater than 10 nm is best for the RVM (at 115 nm instead of 105 nm). Most importantly, however, the computed entrance and exit hysteresis loops agree closely for the DVPM, but are almost non-existent for the RVM. The deformation allowed by the DVPM permits the vortex to move ahead into the site, and linger in the site at a lower energy cost than the rigid model.

Disk sizes between 500 nm diameter/40 nm thick and 2000 nm diameter/20 nm thick were simulated with identical M_S variation pinning sites (Fig. 9). The DVPM was found to give good estimates of hysteresis width and vortex position for all disk sizes when an optimized value of R_1 was used. For disks significantly larger than 1 μm in diameter, at 40 nm thickness, the pinned magnetic differential susceptibility was found to be underestimated. Fig. 9 shows a 500 nm and 1500 nm diameter result for comparison.

The value of R_1 used makes a significant difference in computing pinning effects in comparison to unpinned behavior. Changing R_1 has a weak influence on the computed m–h and s–h curves, mitigated by the coupling approach used to modify the shell demagnetization factor. More importantly, the value R_1 dictates the energetic cost of displacing the core via the exchange-demagnetization spring. Reducing the proportional value of R_1 stiffens the spring. This in turn has a significant effect on pinning and depinning barriers. In the previous section, errors between the DVPM and its component models were analyzed to determine the optimal R_1, providing an R_1 estimate independent of simulations. In the case of pinning, however, no model is adequate for comparison, and consequently it is worthwhile to compare the computed optimal R_1 to values empirically extracted by comparison to well-defined pinning simulations. As in the comparison
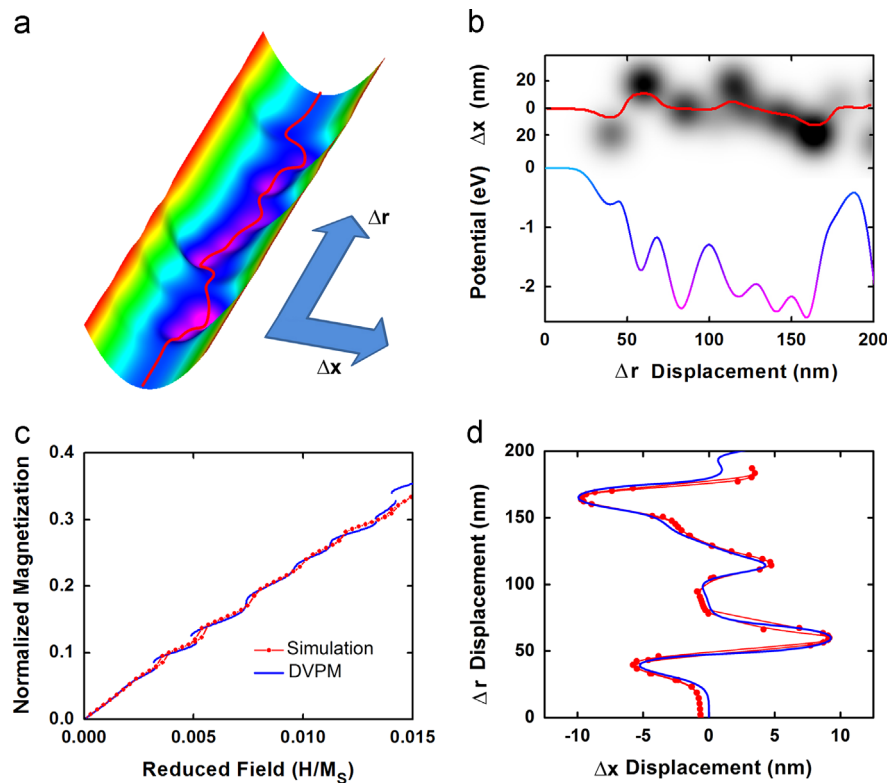
Fig. 10. (a) A 3-D plot shows the pinning site potential combined with the harmonic potential for deviations orthogonal to the path defined by the applied field. The computed path of minimum energy, $\Delta x(\Delta r)$ is plotted as a red thread. (b) At top the 2-D pinning potential is plotted with the computed minimum energy path (red line). Below, the equivalent 1-D potential is presented. The equivalent potential incorporates contributions from both the pinning potential and harmonic trough. The color gradient on the potential line matches the color scale in panel (a). (c) The magnetization curve computed from the potential in (b) is compared against a simulated curve incorporating M_S suppressed regions with the same 2-D distribution. The depth of the 2-D potential used in the model calculations is estimated from the simulation. Agreement is very close, though some deviations show up as the vortex displacement increases and a large energy change is encountered. (d) The simulated $\Delta x(\Delta r)$ is compared to the computed minimum path, showing excellent agreement. (For interpretation of the references to color in this figure caption, the reader is referred to the web version of this article.)

made to the RVM and TVM, in general the value $R_1 = R/2$ provides reasonable results for a variety of disk sizes. However, for disks below 1 μm in diameter (for 40 nm thickness), reduced R_1 values provide better pinning performance, particularly in estimated hysteresis width, reflecting the increasing rigidity of smaller disks. A comparison between the optimal R_1 values computed by error minimization against the RVM and TVM, and also by comparison with simulation, is shown in the inset of Fig. 8d. Each optimization method returns the same trend of decreasing R_1/R with the value of R in close agreement with one another for disks 1 μm in diameter and below. For large and thin disks, $R_1 = R/2$ provides better agreement with simulation. This reflects the fact that in low aspect ratio disks that are very large compared to the exchange length, the character of flexing in the magnetization distribution will change to include more complex deformations beyond the scope of the TVM approximation used.

For experimental or analytic situations where complementary simulation is not possible, the R_1 obtained at the end of the theory section from error minimization against the RVM and TVM predictions for ideal disks provides a reasonable estimate. Whenever it is possible, constructing a simulation of a disk with the desired radius and thickness with a single, simple pinning site, and extracting the optimal R_1 value is preferable. It should be noted that for a given disk aspect ratio, once the optimal R_1 is computed from a single simulation, the R_1 value is then fixed. Thus far, we have noted that no dependence of R_1 on the size, shape or strength of the pinning sites incorporated into our simulations. These include pinning sites ranging from 10 nm to 50 nm in diameter, with relative M_S suppression between 0 and 85%, and featuring

either sharp or gradual edges in the pinning potential. Once the R_1 value is fixed, the model permits computation of the effects of arbitrary pinning potentials or even fitting magnetization curves to extract information about the pinning potentials.

3.3. Two dimensional pinning potentials

The DVPM provides excellent performance in the description of ideal disk behavior and pinning for idealized simulations. However, in application to real samples, inclusion of pinning sites directly along the usual (no pinning) path followed by the vortex is limiting. As noted in recent numerical simulation work on pinning [37], a more realistic case is to consider pinning sites near, but not centered on, the field-defined path. This can be incorporated into the 1-D model presented here by computing the 1-D equivalent potential of the actual 2-D path followed by the vortex. Deviations orthogonal to the path defined by the applied field have an energy cost approximated by $\kappa \Delta x^2$ where the value of κ is given by Eq. (4). Since the magnetization induced by these deviations is orthogonal to the applied field, the energy is effectively static and can be summed with a 2-D distribution of pinning sites to form a trough guiding the vortex through the 2-D energy landscape. It is then possible to compute the minimum energy pathway $\Delta x_o(\Delta r)$ that the vortex will follow as it is deflected (Fig. 10a). Computing the total static energy, pinning plus the trough energy, $E(\Delta x_o)$ yields an equivalent 1-D potential as a function of Δr (Fig. 10b). This potential can then be summed, as the Gaussian pinning sites were previously, with the potential for a perfect disk including field.

Solving for minima as before allows computation of the evolution of the magnetization and vortex position in the 2-D potential.

This approach is applied to a simulation that incorporates a 2-D distribution of 20 nm diameter pinning sites with various values of suppressed M_S near the field-defined path. As before, the pinning sites are incorporated into the model as Gaussian wells with depths estimated from the simulation and profiles computed by convolving a Gaussian with the profile of the M_S variation. The computed 2-D path agrees well with the vortex position extracted from simulation, as does the computed magnetization (Fig. 5c and d). Some disagreement is noted as the deflection increases close to the effective $R/2$ limit of the model, and the vortex passes over a large barrier. In this computation, a sparse 2-D distribution of sites ensures a unique $\Delta x_o(\Delta r)$, however, in principle this approach can be extended to bistable states in Δx by consideration of multiple vortex tracks. Computation of the energy barriers separating tracks, however, would require a more complete minimization over 4-D space with two RVM displacements and two TVM displacements.

4. Conclusion

The piecewise approach applied to develop the DVPM yields a highly functional analytic model that makes quantitatively accurate predictions of a wide variety of properties of a vortex in a disk. Most notably, it provides a powerful description of vortex core pinning and provides greater physical insight into the behavior of the vortex during pinning. It is important to note that the pinning potentials extracted from simulations, and subsequently added to the model represent the total magnitude of the interaction of the vortex core with the pinning sites. This implicitly includes the energetic cost of core deformations, which are not treated directly by the model. However, since skirt deformations are included explicitly, the cost of core distortions and core interactions may be isolated and studied in detail. This highlights the practical purpose of the model: in order to accurately study the core and its behavior during pinning, the dominant influence of the skirt must be explicitly accounted for. The DVPM constitutes a tool capable of doing this, and consequently elevating empirical magnetization data to a quantitative probe of vortex core interactions. The model holds promise as a tool in probing the modification of pinning in technologically pertinent thin films to better understand effects such as ion damage. The piecewise approach demonstrated may, in future, be generalized to other geometries, permitting quantitative computation of device behavior without cumbersome simulation.

Acknowledgments

References

[1] R.P. Cowburn, D.K. Koltsov, A.O. Adeyeye, M.E. Welland, D.M. Tricker, Phys. Rev. Lett. 83 (1999) 1042–1045.
[2] T. Shinjo, T. Okuno, R. Hassdorf, K. Shigeto, T. Hono, Science 289 (2000) 930.
[3] S.S.P. Parkin, M. Hayashi, L. Thomas, Science 320 (2008) 190–194.
[4] N.A. Usov, S.E. Peschany, J. Magn. Magn. Mater. 118 (1993) L290–L294.
[5] A. Wachowiak, J. Wiebe, M. Bode, O. Pietzsch, M. Morgenstern, R. Wiesendanger, Science 298 (2002) 577.
[6] B.E. Argyle, E. Terrenzio, J.C. Slonczewski, Phys. Rev. Lett. 53 (1984) 190.
[7] J.P. Park, P. Eames, D.M. Engebretson, J. Berezovsky, P.A. Crowell, Phys. Rev. B 67 (2003) 020403.
[8] S.B. Choe, Y. Acremann, A. Scholl, A. Bauer, A. Doran, J. Stöhr, H.A. Padmore, Science 304 (2004) 420.
[9] V. Novosad, K.Y. Guslienko, H. Shima, Y. Otani, K. Fukamichi, N. Kikuchi, O. Kitakami, Y. Shimada, IEEE Trans. Magn. 37 (2001) 2088.
[10] J.A.J. Burgess, D.C. Fortin, J.E. Losby, D. Grombacher, J.P. Davis, M.R. Freeman, Phys. Rev. B 82 (2010) 144403.
[11] J.P. Davis, D. Vick, J.A.J. Burgess, D.C. Fortin, P. Li, V. Sauer, W.K. Hiebert, M.R. Freeman, New J. Phys. 12 (2010) 093033.
[12] G. Mihajlovic, M.S. Patrick, J.E. Pearson, V. Novosad, S.D. Bader, M. Field, G.J. Sullivan, A. Hoffmann, Appl. Phys. Lett. 96 (2010) 112501.
[13] G.N. Kakazei, M. Ilyn, O. Chubykalo-Fesenko, J. Gonzalez, A.A. Serga, A.V. Chumak, P.A. Beck, B. Laegel, B. Hillebrands, K.Y. Guslienko, Appl. Phys. Lett. 99 (2011) 052512.
[14] D. Toscano, S.A. Leonel, R.A. Dias, P.Z. Coura, B.V. Costa, J. Appl. Phys. 109 (2011) 076104.
[15] T. Uhlig, M. Rahm, C. Dietrich, R. Höllinger, M. Heumann, D. Weiss, J. Zweck, Phys. Rev. Lett. 95 (2005) 237205.
[16] R.L. Compton, P.A. Crowell, Phys. Rev. Lett. 97 (2006) 137202.
[17] R.L. Compton, T.Y. Chen, P.A. Crowell, Phys. Rev. B 81 (2010) 144412.
[18] T.Y. Chen, A.T. Galkiewicz, P.A. Crowell, Phys. Rev. B Rapid Commun. 85 (2012) 180406.
[19] T.Y. Chen, C. Erickson, M.J. Leighton, P.A. Crowell, 2012. arXiv:1201.1334.
[20] J.S. Kim, O. Boulle, S. Verstoep, L. Heyne, J. Rhensius, M. Kläui, L.J. Heyderman, F. Kronast, R. Mattheis, C. Ulysse, G. Faini, Phys. Rev. B 82 (2010) 104427.
[21] F.A. Apolonio, W.A. Moura-Melo, F.P. Crisafuli, A.R. Pereira, R.L. Silva, J. Appl. Phys. 106 (2009) 084320.
[22] J.A.J. Burgess, A.E. Fraser, F.F. Sani, D. Vick, B.D. Hauer, J.P. Davis, M.R. Freeman, Science 339 (2013) 1051.
[23] A. Aharoni, J. Appl. Phys. 68 (1990) 2892.
[24] W. Scholz, K.Y. Guslienko, V. Novosad, D. Suess, T. Schrefl, R.W. Chantrell, J. Fidler, J. Magn. Magn. Mater. 266 (2003) 155.
[25] K.Y. Guslienko, V. Novosad, Y. Otani, H. Shima, K. Fukamichi, Phys. Rev. B 65 (2001) 024414.
[26] K.Y. Guslienko, V. Novosad, Y. Otani, H. Shima, K. Fukamichi, Appl. Phys. Lett. 78 (2001) 3848.
[27] K.L. Metlov, K.Y. Guslienko, J. Magn. Magn. Mater. 242 (2002) 1015.
[28] K.Y. Guslienko, K.L. Metlov, Phys. Rev. B Rapid Commun. 63 (2001) 100403 (R).
[29] K.Y. Guslienko, B.A. Ivanov, V. Novosad, Y. Otani, H. Shima, K. Fukamichi, J. Appl. Phys. 91 (2002) 8037.
[30] K.S. Buchanan, M. Grimsditch, F.Y. Fradin, S.D. Bader, V. Novosad, Phys. Rev. Lett. 99 (2007) 267201.
[31] K.Y. Guslienko, R.H. Heredero, O. Chubykalo-Fesenko, Phys. Rev. B 82 (2010) 014402.
[32] C. Kittel, Rev. Mod. Phys. 21 (1949) 541.
[33] S. Chickazumi, Physics of Ferromagnetism, 2nd edition, Oxford University Press, 1997.
[34] D.X. Chen, E. Pardo, A. Sanchez, J. Magn. Magn. Mater. 306 (2006) 135.
[35] K.L. Metlov, Phys. Rev. Lett. 105 (2010) 107201.
[36] A.A. Thiele, Phys. Rev. Lett. 30 (1973) 230.
[37] G.M. Wysin, J. Phys.: Condens. Matter 22 (2010) 376002.